A Fourier Transform Spectrometer for Ground Testing of the Herschel/SPIRE Instrument

Locke D. Spencer[a], David A. Naylor[a], Bruce M. Swinyard[b], Asier A. Aramburu [b], Trevor R. Fulton[a], Tanya L. Lim[b], Samuel D. Ronayette[b], and Ian S. Schofield[a]

[a]Department of Physics, University of Lethbridge, Alberta, Canada;
[b]Rutherford Appleton Laboratory, United Kingdom

ABSTRACT

The Spectral and Photometric Imaging Receiver (SPIRE) is one of three instruments on the European Space Agency's Herschel mission. A detailed understanding of the SPIRE instrument is essential for a successful mission. In particular, it is important to characterize both the in-band spectral profile, and any out-of-band spectral leaks, which would severely degrade performance. A test Fourier Transform Spectrometer (TFTS), with its broad spectral coverage and intermediate spectral resolution, was selected for the spectral characterization of SPIRE. The integration of the TFTS with the existing Ground Support Equipment of the Herschel/SPIRE test facility at the Rutherford Appleton Laboratory imposed several mechanical, optical, electrical, and software constraints. In this paper we describe the design and implementation of the TFTS, and present preliminary results from its use in the SPIRE verification and performance tests.

Keywords: Herschel, SPIRE, Far-infrared, Fourier Transform Spectrometer, Spectral characterization

1. INTRODUCTION

The main scientific objectives of the Herschel mission are spectroscopy of star forming regions in our own and nearby galaxies, and deep extragalactic and galactic imaging surveys.[1] Herschel will be the only space facility dedicated to observing one of the last unexplored bands of the electromagnetic spectrum.[2] The Herschel telescope has a 3.5 m primary mirror passively cooled to ∼80 K. The Spectral and Photometric Imaging Receiver (SPIRE) is one of Herschel's three focal plane instruments. SPIRE consists of a three band imaging photometer and a dual band imaging Fourier Transform Spectrometer (FTS). To achieve high sensitivity, SPIRE is cooled to ∼11K and the detector arrays operate at 300 mK.[3] The import ant features of SPIRE are summarized in Table 1.

The combination of a low emissivity, passively cooled telescope, the total absence of atmospheric emission, and a cryogenically cooled payload will allow sensitive photometric observations. SPIRE is designed to operate in the absence of an atmosphere and the SPIRE instrument itself is inside an evacuated cryostat during testing to simulate space flight conditions. Outside of the cryostat, however, ground testing occurs under atmospheric conditions. The test facility consists of a molecular laser to provide an accurate line source and a blackbody source for beam profiles. A spectrometer was identified as an additional piece of test equipment required to determine the spectral performance of SPIRE. The SPIRE test FTS (TFTS), with its broad spectral coverage, intermediate and variable resolution, intrinsic wavelength and intensity calibration, and simplicity of integration was designed for this task. The TFTS was provided by the University of Lethbridge Astronomical Instrumentation Group (AIG), under contract to the Canadian Space Agency (CSA) as part of Canada's official contribution to the Herschel/SPIRE project.

The design of the TFTS is presented in Sec. 2. Pre-vibration verification testing is discussed in Sections 3 and 4 with results presented in Sec. 5. Section 6 discusses future test plans. More details of the current status of the SPIRE instrument can be found elsewhere.[4–6]

locke.spencer@uleth.ca; telephone (403) 329 2719; fax (403) 329 2057; www.uleth.ca/phy/naylor

Parameter	Photometer	Spectrometer
Spectral Bands [μm]	250, 300, 500	200 - 315, 315 - 670
Resolving Power	3	1000
Number of Pixels	43, 88, 139	19, 37
Field of View	4' x 8'	2.6' diameter

Table 1. Comparison of the Photometer and Spectrometer components of SPIRE

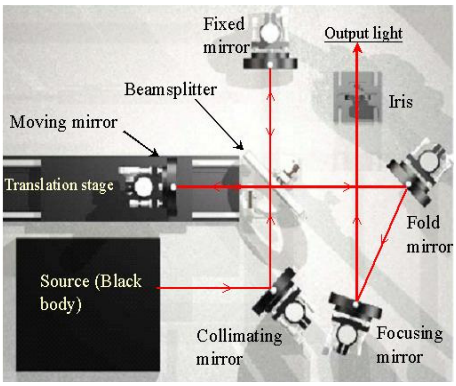

Figure 1. Herschel/SPIRE qualification TFTS with Blackbody radiation source. The TFTS is in a sealed enclosure to allow humidity control. Dimensions are 1m x 0.7 m.

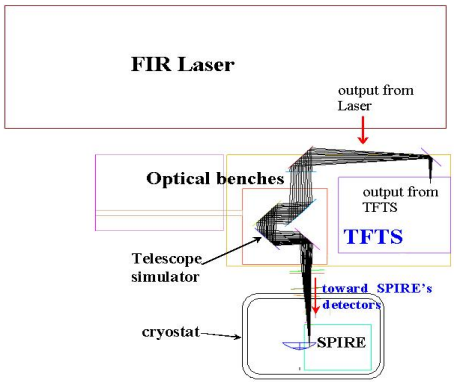

Figure 2. Herschel/SPIRE AIV facility equipment diagram including TFTS. The optical path between the TFTS output port and the cryostat window are also in a sealed enclosure to allow for humidity control. The area shown is approximately 3.5m x 4m.

2. TEST FOURIER TRANSFORM SPECTROMETER DESIGN

Several performance requirements influenced the TFTS design. The baseline requirement of the TFTS is that it provide a resolution of 0.5 cm^{-1} (i.e., a resolving power greater than 1000 at 200 μm) and fit within mass and volume constraints (see Table 2). The goal was to produce the highest possible resolution within these constraints. These requirements fell into mechanical, optical, electrical, and software categories. We discuss each of these in detail.

2.1. TFTS mechanical Constraints

The need for the TFTS was not addressed until after the Assembly Integration Verification (AIV) facility at the Rutherford Appleton Laboratory (RAL) was already in place; this restricted the choice of the TFTS design. Fig. 2 shows the SPIRE test facility layout. In addition to the bulky SPIRE cryostat, the laboratory includes a telescope simulator, molecular laser, and blackbody calibration source, all mounted on several large optical tables. Due to the TFTS's location near the edge of a large optical bench there was a mass constraint. The TFTS also needed to be in an enclosed volume to allow humidity control in the beampath. The TFTS outline is shown in Fig. 1 and makes very efficient use of the space available.

2.2. TFTS Optical Constraints

In order to test the SPIRE instrument it is necessary to simulate a beam identical to that provided by the Herschel telescope. This was accomplished by a telescope simulator constructed from four mirrors (three flat, one powered), three of which are motorized. These mirrors are significantly smaller than the Herschel primary mirror which is simulated ($\sim$30 cm vs. 3.5m diameter). A point source located at the input of the telescope

simulator can be focused on any detector by adjusting the motorized mirrors in such a way as to simulate the curved field of the Herschel telescope. The pupil mask, with image located 2.64 m from the SPIRE focal plane, reproduces the F/8.68 beam required by SPIRE. Thus any of the SPIRE bolometers can be illuminated by a point source similar to that provided by the Herschel telescope optics. The Telescope simulator design is discussed in greater detail in Collins *et al*, 2003.[7]

As shown in Fig. 1, the TFTS provides the telescope simulator with an F/8.68 beam by a series of powered mirrors. The blackbody source is located at the focus of an F/2.33 collimating mirror (off-axis parabolic, focal length 17.48 cm). The collimated beam enters the interferometer where it encounters the beamsplitter, and fixed and moving mirrors. The beam exits the interferometer and after reflection off a plane mirror is brought to a focus by an F/8 mirror (focal length 60 cm) which feeds the telescope simulator. An iris that is located at this focus provides a field stop for the radiation that is modulated by the interferometer. The use of an off-axis parabola, fold, and focal compression mirrors makes the most of the limited surface area of the optical table.

The TFTS employs a broadband, high-efficiency, intensity beamsplitter[8] identical to that used in SPIRE. Throughput is a factor of 2 higher than it would be for the traditional polarizing beam dividers as there is no sensitivity to the polarization of the incident radiation. Another feature of the TFTS is the beamsplitter mount, which allows for rapid beamsplitter exchange while preserving the alignment. During initial setup a thin Mylar beamsplitter is used for visible alignment of the interferometer itself, and also of the interferometer with the telescope simulator. The optical alignment of the TFTS and telescope simulator requires the alignment of fourteen optical components, a task made significantly easier working in the visible range.

2.3. TFTS Electrical Constraints

In Fourier transform spectroscopy, the interferogram, $I(z)$, (where z is the optical path difference between the interfering beams) is related to the source spectrum, $B(\sigma)$, (where σ is the frequency in wavenumbers) by:

$$I(z) = \int_{-\infty}^{+\infty} B(\sigma) e^{-i2\pi\sigma z} d\sigma \tag{1}$$

This equation can be inverted to retrieve the spectrum.[9] It is common practice to measure the interferogram in equal increments of optical path difference, which allows use of the FFT algorithm. For the TFTS/SPIRE system, the interferogram signal is recorded as a function of time, $I(t)$, and the time of the regular optical path difference intervals, $t'(z)$, is recorded independently. By combining $I(t)$ and $t'(z)$ it is possible to reconstruct $I(z)$ (spatial domain) and hence retrieve the spectrum, $B(\sigma)$ (spectral domain).

The TFTS employs a precision linear motion translation stage which eliminates pitch and yaw errors associated with lead-screw type stages. The stage also provides positional information at the level of ± 10 nm by means of a noncontact linear encoder and multiplier option (AEROTECH model ALS135-200). The encoder Position Synchronized Output signal (PSO) triggers time capture on the Digital Processing Unit (DPU) electronics, whereby the time stamp is stored in a 64-slot, 32 bit FIFO. The TFTS was designed primarily for a rapid-scan mode, in which the times at which the stage advances equal intervals of optical retardation are recorded, $t'(z)$, while the mirror scans at a constant velocity either towards or away from the beamsplitter (up and down scans, respectively). A counter which increments at the DPU clock frequency of 312.5 KHz, and is synchronized with the SPIRE instrument, is needed to allow for accurate interpolation.

$$\begin{matrix} I(t) \\ t'(z) \end{matrix} \Rightarrow I(z) \tag{2}$$

Equation 2 illustrates the interpolation of the time sampled interferogram signal, $I(t)$, and the position sampled optical retardation times, $t'(z)$, to yield the interferogram, $I(z)$. The DPU clock signal is part of the SPIRE electronics, with which direct access was prohibited, hence a breakout box (see Fig. 3) was proposed as a potential solution. The breakout box provides an interface between the SPIRE Detector Control Unit (DCU) and SPIRE Digital Processing Unit (DPU) clock. The SPIRE and TFTS sections of the breakout box are electrically isolated from one another to ensure that malfunctions in the TFTS cannot adversely affect the SPIRE instrument. In addition to the DPU clock pulses, the breakout box also recognizes global electronics

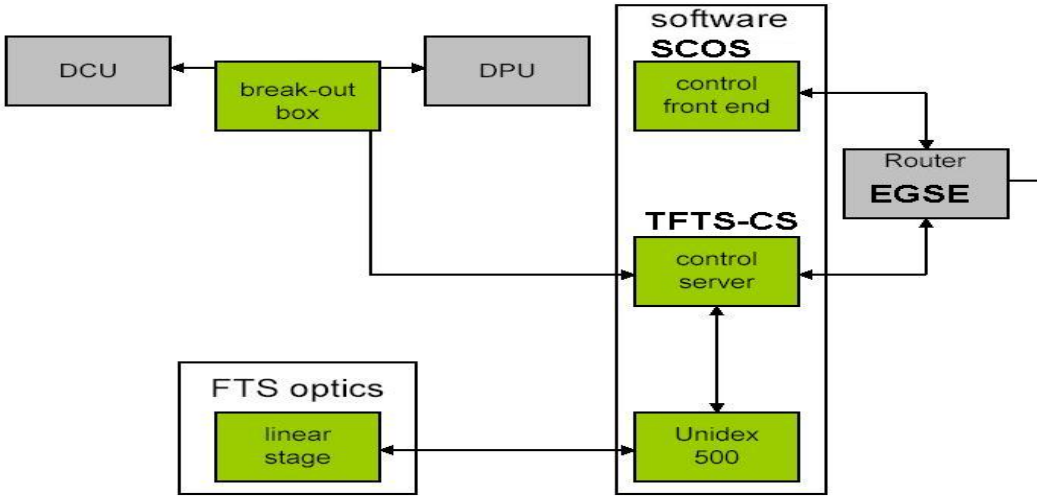

Figure 3. Block diagram outlining link between the TFTS, TFTS-CS, and SPIRE through the breakout box.

resets which allow the two clock counters , t and t' (i.e. the bolometer readout clock counter and the TFTS clock counter) to be synchronized to within 100 ns, well below the packet time uncertainty for the bolometer readout of 1 μs.[10]

As a check of the breakout box assisted time synchronization the interferometer should return the same zero path difference (zpd) position value independent of scan direction. Sec. 5.1 shows that preliminary data analysis indicated that the zpd location reported for both scan directions was not the same. The difference between up and down scan zpd's is equivalent to an 80 ms time delay between reported bolometer signal values and stage position values. The cause of this difference has been identified and the exercise served as a useful check to ensure that the synchronization between the time sampled SPIRE bolometer signal and the TFTS stage position time was functioning correctly.

2.4. TFTS Software Constraints

The TFTS Control Server (TFTS-CS) is a Windows 2000 based network server application that configures, controls, and collects data from the TFTS. Communication via an Ethernet-based Local Areal Network (LAN) uses ESA's Electrical Ground Support Equipment (EGSE) data packet protocol. The TFTS-CS accepts instruction packets, executes the instructions contained in the packets, and returns data packets if applicable. The software is event driven, and multi-threaded, to perform background operations simultaneously - such as scanning and housekeeping packet broadcasting. Specifically, separate threads of execution handle regular transmission of housekeeping packets as well as performing long-duration functions such as scans and table motion. Inter-thread communication is implemented with global variables, protected by critical section functions. Network activity, or button presses, trigger the TFTS-CS. Critical interfaces for the TFTS-CS are shown in Fig. 3 and include: EGSE router, Spacecraft Operating System (SCOS), and DPU counter electronics, all linked together through the breakout box, and external hardware specific to the TFTS which is responsible for the position and time capture.

Since there are 5 different arrays of detectors to be evaluated and characterized, the TFTS has been designed for flexibility. Variable scan speed, sampling rate, and maximum optical path difference enable a wide variety of spectral observation parameters (see Table 1).

3. TESTING OF THE SPIRE CRYOGENIC QUALIFICATION MODEL

Vibration testing is carried out to simulate the conditions the Herschel satellite will experience during launch. Pre vibration tests provide a benchmark for comparison with post-vibration and future instrument testing.

Parameter	Typical	Range
Input F Number	F/2.33	N/A
Output F number	F/8.68	N/A
Resolution	0.0125 cm^{-1}	0.0125 - 0.25 cm^{-1}
Physical Dimensions	1m x 0.75m x 0.3m	N/A
Nyquist Frequency	100 cm^{-1}	10 - 50000 cm^{-1}
Mirror velocity	0.5 mm/s	0.01 - 5 mm/s
TFTS enclosure humidity	6 %	1 - 30%
Blackbody Temperatures	1200^{o}C	150 - 1300^{o}C
Mass	~100 kg	N/A

[a] see Eqn. 4

Table 2. Summary of SPIRE Test FTS Capabilities

Performance changes, if any, should be fully understood to ensure that the instrument has not been affected by the vibration tests. The multiple detector arrays and test phases also imply a need for testing to be repeatable and flexible. Ground based testing of the SPIRE instrument poses challenges in simulating the deep space environment that gives SPIRE its observational advantages. A multi-stage Helium cryostat cools SPIRE to the required temperatures (77K, 11K, 0.3K). Cryogenic qualification model (CQM) testing is comprised of two stages, pre-vibration testing, and post-vibration testing. Volume limitations also pose an obstacle to instrument verification. For current information that discusses more general aspects of SPIRE CQM verification testing refer to Lim *et al*, 2004.[4]

Significant obstacles to CQM testing are the atmospheric conditions outside of the cryostat. The chief obstacle caused by the atmosphere is the opacity in the SPIRE spectral band due to atmospheric water vapor. Fig. 4 shows the atmospheric transmission of both the photometer (PLW, PMW, PSW) and spectrometer (SLW, SSW) bands for a 5m path at various relative humidities under laboratory conditions.[11] Only the PLW array was available for CQM testing. The atmospheric transmission across the PLW band has fairly low opacity with a strong water absorption line at 18.578 cm^{-1}. This absorption line is useful for intensity and wavelength calibration. The high transmission region between 19 and 24 cm^{-1} provides higher signal-to-noise data which in turn allows reliable broadband phase correction. The PLW array is therefore seen to be a good choice for CQM testing because of these simple atmospheric properties. Fig. 4 also illustrates the greater atmospheric opacity for wavenumbers above 36 cm^{-1}. Serious attempts at purging the atmospheric water vapour from the beampath will be required to reduce opacity to an acceptable level for CQM testing of the short wavelength arrays.

3.1. Parameter Selection

During CQM testing, test parameter selection involved a compromise between different test goals. Four variables are free to be manipulated to obtain the desired spectral properties: TFTS stage velocity , TFTS position sampling interval, hot blackbody temperature, and maximum optical path difference (opd_{max}). Given the limited amount of time allotted to the TFTS during the test campaign the fundamental trade off lies between signal-to-noise and spectral resolution. In total 9 pixels were tested at a variety of scan speeds, resolutions, and blackbody temperatures. Observing parameters are shown in Table 3. The choices in setting these parameters in the case of the PLW array are discussed below.

3.1.1. Stage Velocity

The TFTS stage velocity is dictated by the bolometer rolloff frequency (5 Hz). The relationship between stage velocity, spectral content, and the maximum interferogram frequency observed by the detectors, f in Hz, is given by

$$f = 2v\sigma_{max} \qquad Hz \tag{3}$$

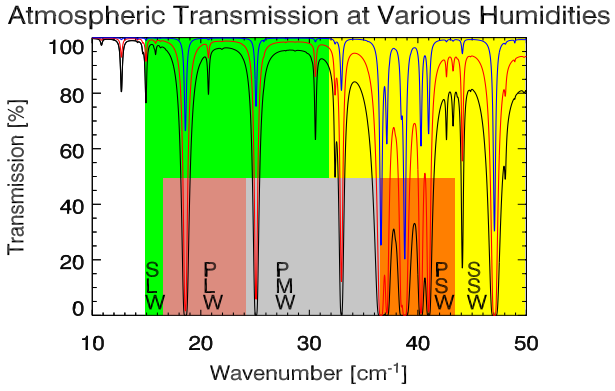

Figure 4. Atmospheric transmission at various relative humidities for the test facility FTS beampath of 5.092 m.[11] Humidities shown are (top to bottom) 1%, 10%, and 30%. 30% is easily achieved, 10% is a challenge, and 1% is very difficult to achieve.

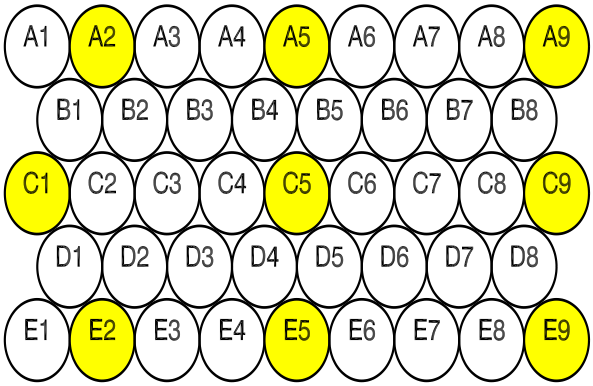

Figure 5. Array Structure for the Photometer Long Wavelength (PLW) Array. Pixels tested in the pre-vibration test campaign are shaded.

where σ_{MAX} is the maximum frequency, in cm^{-1}, seen by the detector and v is the linear stage velocity in cm/s. In the case of the PLW band, the highest frequency is on the order of 25 cm^{-1} which dictates a stage velocity no greater than 1.0 mm/s. A velocity of 0.5 mm/s was selected.

3.1.2. Sampling Interval

From information theory, the maximum observable or Nyquist frequency, σ_N in cm^{-1}, is given by the equation:

$$\sigma_N = \frac{1}{2\Delta z} \qquad cm^{-1} \tag{4}$$

where Δz is the optical sampling interval in cm. The stage position is sampled every 25 μm of stage travel, resulting in a Nyquist frequency of 100 cm^{-1}. This value four times oversamples the PLW band and will twice sample the shortest frequency in any SPIRE array. The stage is capable of sampling on a much finer level, however, given the out-of-band rejection of the SPIRE instrument this is unnecessary.

3.1.3. Spectral Resolution / Maximum Optical Path Difference

The Spectral Resolution is determined by the opd_{max} and is given by:

$$\Delta\sigma = \frac{1.207}{2opd_{max}} \qquad cm^{-1} \tag{5}$$

As mentioned above, there is a direct trade off between spectral resolution and signal-to-noise ratio. In the case of the PLW array, the minimum required resolution, based on the absorption line width and desired band edge profile resolution, is 0.3 cm^{-1}.

3.1.4. Blackbody Scan Temperature

The signal-to-noise levels of the interferogram increase with blackbody temperature. As discussed in Sec. 5.3, spectral measurements of the blackbody at two different temperatures, ideally widely spaced, are required to determine the Spectral Responsivity. During the test campaign, the blackbody was operated at 1200^{o}C and 950^{o}C. This was a reasonable compromise in that both temperatures are well above ambient and yet a significant difference exists between them.

To maximize the number of pixels that could be measured, it was decided to conduct low and full resolution scans at two blackbody temperatures for the central pixel, and do low resolution scans at one blackbody temperature (1200^{o}C) on the other pixels to be tested (see Table 3). This allows more pixels to be tested and better signal-to-noise in the given time.

Pixel	Stage Velocity [mm/s]	opd_{max} [cm]	Δz [μm]	BB[a]Temp. [^{o}C]	Humidity [%]	Scan Pairs
A2	0.5	2	25	1200	7.8	6
A5	0.5	2	25	1200	7.8	6
A9	0.5	2	25	1200	7.0	6
C1	0.5	2	25	1200	10.0	6
C5	1.0	2	25	1200	10.5	60
C5	1.0	2	25	950	8.0	60
C5	0.5	34	25	1200	7.5	6
C5	0.5	34	25	990	8.7	6
C9	0.5	2	25	1200	5.6	6
E2	0.5	2	25	1200	12.0	6
E5	0.5	2	25	1200	6.0	6
E9	0.5	2	25	1200	6.0	6

[a] Blackbody Radiation Source

Table 3. TFTS Tests Performed during pre-vibration SPIRE CQM Verification

4. DATA ANALYSIS

CQM test data were extracted from the EGSE database using a Jython script that called Java routines from the SPIRE Interactive Quick Look Analysis software package. The telemetry from the photometers, in the form of a timeline, was written to one file, while nominal science data (mirror-position timeline) from the TFTS was written to another file. Each file was written in the FITS format[12] and conformed to the standard outline in the University of Lethbridge Data Processing Toolkit (DPTK) Architecture Design Document (ADD).[13]

The DPTK is a set of data processing routines written in the Interactive Data Language (IDL).[14] The processing pipeline begins by combining the timelines contained in the two FITS files. The combined timeline is then subdivided into discrete software objects, with each object containing one scan. The data in each scan timeline are then used to create a series of interferogram objects by way of interpolation as discussed in Sec. 2. The interferograms are converted into spectra by application of standard Fourier spectroscopic techniques, which consist of phase correction, optional apodization, and Fourier transformation.[15]Phase correction can be implemented in either the spatial or spectral domain. For low resolution scans, in which the interferogram is measured out to equal distances on both sides of the zpd position, the phase correction is implemented in the spectral domain. For high resolution scans, which lack this symmetry, phase correction is implemented in the spatial domain. Optional apodization can be applied the the interferogram prior to Fourier transformation to reduce the magnitude of the sidelobes of the instrumental line shape, albeit at the cost of lower resolution.[15] From the perspective of the DPTK, the end result is that a series of interferogram objects is transformed into a series of spectrum objects.

5. RESULTS

Four main results arise from the TFTS CQM campaign: the performance of the TFTS, the comparison of the observed spectrum with theory, a detailed analysis of the spectral responsivity of the central pixel, and the results for all pixels with comparisons.

5.1. TFTS Performance

As mentioned in Sec. 2, preliminary data analysis indicated that the zpd location differed for the up and down scans; the difference being equivalent to an 80 ms time delay between reported bolometer signal values and stage position values. Since great lengths were undertaken to synchronize the TFTS and SPIRE clocks (less

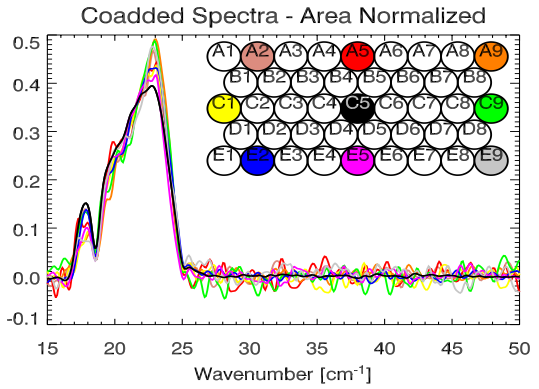

Figure 6. Observed (averaged) spectra from each pixel for the pre-vibration CQM test campaign. Spectra are normalized to pixel C5 by the area under the curve of each spectrum over the high signal-to-noise region.

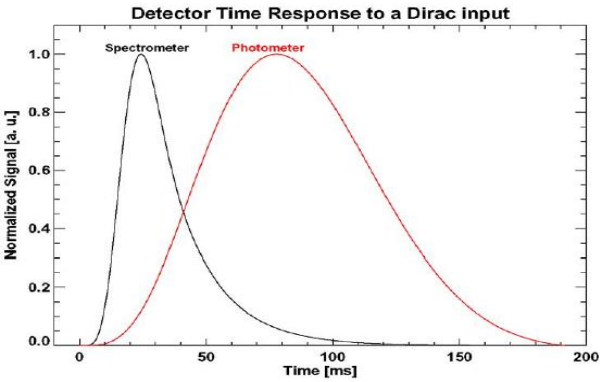

Figure 7. Simulated impulse response to a dirac-delta function for the SPIRE spectrometer and photometer arrays.

than 100 ns) it was clear that some additional delay had not been accounted for. It was quickly realized that the time delay associated with the bolometer time constant and the detector electronics could be the cause. Using subsystem information provided by JPL[16] and LAM,[17] the detectors and their electronics are modeled in Laplacian space and the results for the photometer and spectrometer arrays are shown in Fig. 7. It is readily seen that the 80 ms delay observed agrees with the expected impulse response of the PLW array, thereby validating the SPIRE/TFTS clock synchronization.

The interferometric performance of the TFTS was validated using a molecular laser, a subsystem of the SPIRE test facility. Formic acid has a lasing transition at a wavelength of 432.65 μm (there are actually two closely spaced lines at 432.63 and 432.67 μm of similar strength; this separation is well below the resolution of the TFTS so a mean value was assumed). The molecular laser was filled to a pressure of $\sim$0.2 mbar of formic acid; the molecular laser was pumped by the 9R20 line of CO_2. The CO_2 laser was operating in continuous flow mode with a pressure of $\sim$25 mbar. The optical power in the pump was on the order of $\sim$40 W. The molecular laser was tuned by adjusting the length of the resonant cavity. A pyroelectric detector was used to monitor the power of the infrared signal by means of a beamsplitter placed in the output path of the laser. The exiting beam was then directed towards the TFTS, and by means of a periscope mirror system injected into the TFTS. A Golay cell was placed inside the SPIRE test cryostat and viewed the TFTS through the cryostat window and telescope simulator. This Golay cell was then used to record an interferogram of the laser source. The pyroelectric detector provided automatic gain control of the interferogram signal by monitoring variations in the laser power output. The signal from both detectors was digitized and time stamped using a LabVIEW data acquisition system.[18]

Figure 8 shows the excellent agreement between the measured instrumental line shape and theoretical line shape given by sin(x)/x. With a knowledge of the sin(x)/x function it has been possible to determine the wavelength of the laser line to a small fraction of the resolution of the TFTS. Great accuracy in the wings of the sin(x)/x function validates the TFTS design. This shows that the TFTS and telescope simulator are not apodizing the interferograms, nor are they introducing any significant distortions.

5.2. Predicted Spectra

The theoretical transmission spectrum of the TFTS must first be modeled to allow for comparison with experimental observations. To be accurate, this modeling should include a full radiative transfer analysis of all optical components from the blackbody, through the TFTS, and the optical path including the telescope simulator to the entrance window of the cryostat. As mentioned previously, the water vapour in the atmosphere is problematic since it acts simultaneously as a source of absorption and emission in the optical path. This provided the impetus for enclosing the beampath and purging the water vapour, however residual amounts remain. The radiative transfer is further complicated in that the second input port of the interferometer corresponds to one of

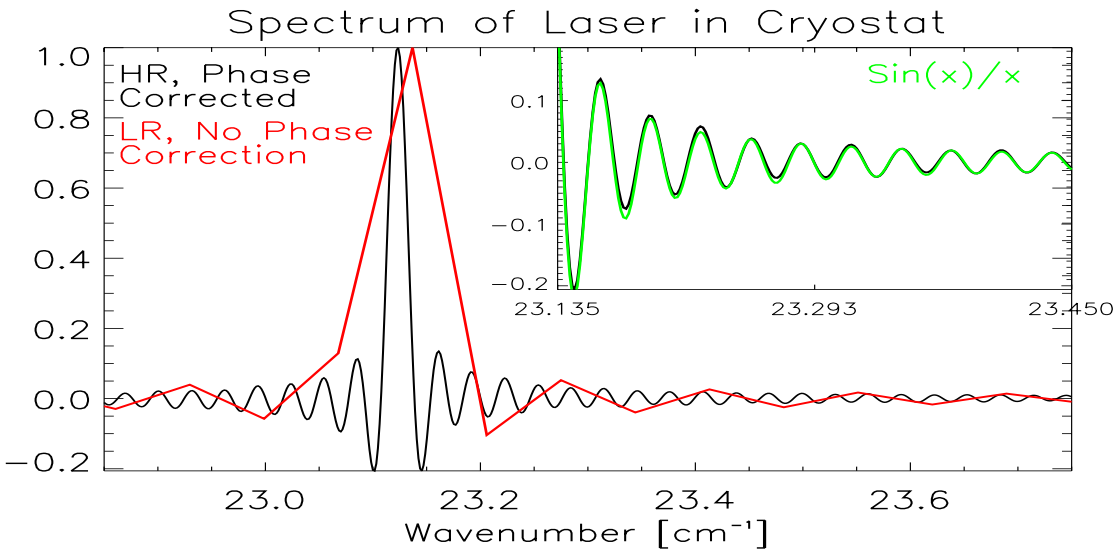

Figure 8. Instrumental Line Shape of the TFTS, telescope simulator, and cryostat window obtained by propagating a laser through the test facility external to SPIRE. Information is shown for both high and low resolution scans. The inset shows a magnified comparison of the TFTS lineshape and classical sin(x)/x function.

the two outputs in the classical Michelson interferometer design; in this case the path from the cryostat window to the TFTS. In addition to the atmosphere there are six mirrors between the cryostat window and the TFTS that act as ambient blackbody sources of unknown emissivity. These sources are not expected to alter the shape of the spectral profile as measurements occur in the Rayleigh-Jeans region and are normalized as part of the analysis. In addition, other detector calibration measures eliminate these uncertainties by using sources inside the cryostat.[4] Therefore, to a first approximation, it was assumed that the theoretical spectrum is given by the following relationship

$$S = F(SR)(\eta)(e^{-\tau})[B_h A\Omega] \tag{6}$$

where F is the filter profile, SR is the spectral responsivity, η is the combined warm mirror efficiency, B_h is the Plank function for the 1200^{o}C blackbody source, $e^{-\tau}$ is the atmospheric transmission, A is the detector area, and Ω is the detector solid angle. $A\Omega$ is expected to be proportional to λ^2 due to the single mode propagation. The expected spectrum for a 1200^{o}C blackbody source seen by the PLW array is shown in Fig. 10, which is based on the assumption that the spectral responsivity is unity.

5.3. Detector Responsivity

Equation 6 is modified by k to account for radiation between the cryostat window and TFTS as mentioned above.

$$S = F(SR)(\eta)(e^{-\tau})[B_h A\Omega - k] \tag{7}$$

The negative sign indicates this spectral contribution originates from the second input port of the Michelson interferometer. The mirror efficiency, η, is assumed to be 0.83 as it represents the reflectivity of six room temperature mirrors (0.97 each). The Spectral Responsivity, SR, can be determined by taking the difference between two spectra (Eqn. 7) obtained at different blackbody temperatures. If external environmental conditions, such as relative humidity, are constant, SR becomes:

$$SR = \frac{S}{F\eta e^{-\tau}[B_h A\Omega - k]} \tag{8}$$

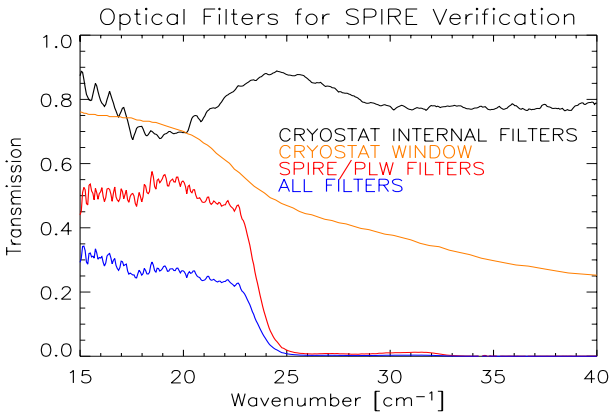

Figure 9. Profiles of optical filters from the cryostat window to the PLW array.

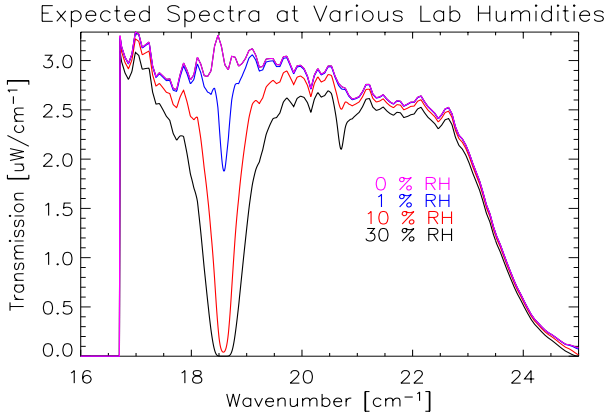

Figure 10. Expected PLW spectrum from a diffraction limited blackbody radiation source at 1200°C and various humidities. This is calculated assuming a Spectral Responsivity of Unity (see Eqn. 6).

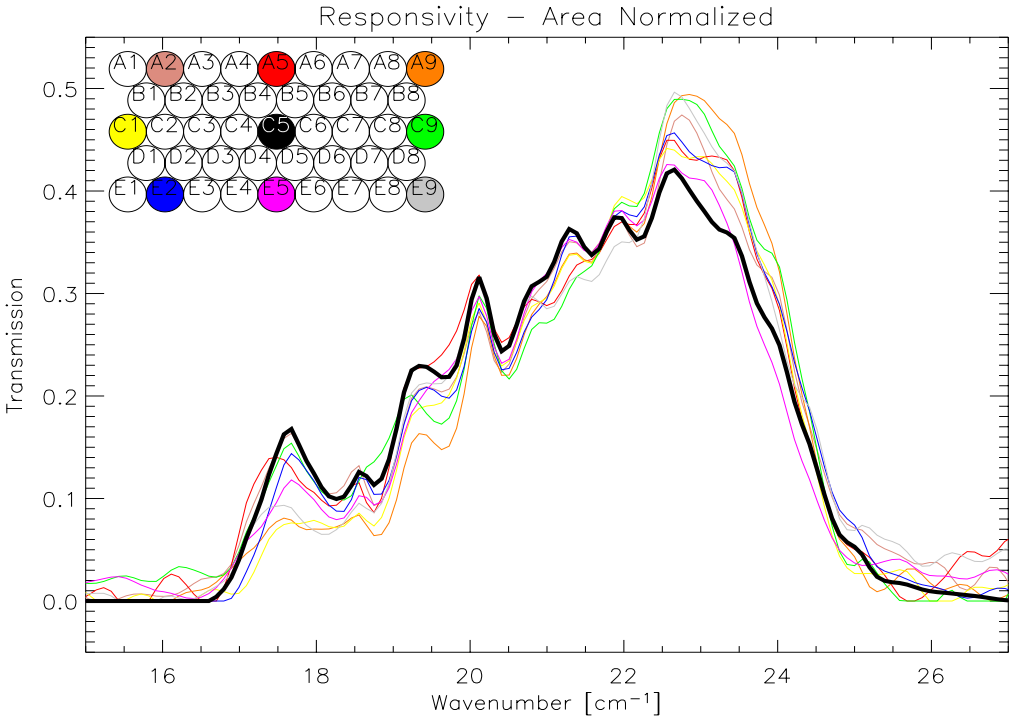

Figure 11. Spectral Responsivity for All Tested Pixels as determined by Eqn. 10.

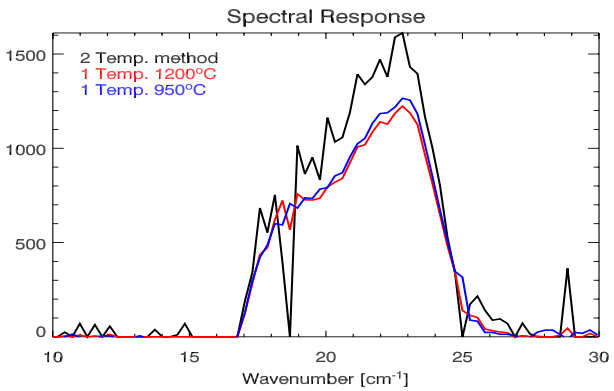

Figure 12. Responsivites determined for central pixel (C5) using both calculation methods (Equations 9 and 10).

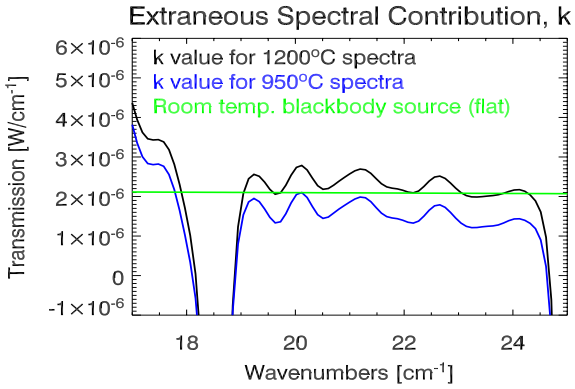

Figure 13. Extraneous spectral source as identified in Eqn. 7 calculated with Eqn. 8 using the spectral response for the central pixel obtained from Eqn. 9. Also shown is a room temperature blackbody source (flat).

$$SR = \frac{S_1 - S_2}{F(\eta)(e^{-\tau})(A\Omega)[B_{h1} - B_{h2}]} \tag{9}$$

Eqn. 9 is used to determine the Spectral Responsivity for the central pixel of the PLW array. In order to measure as many pixels as possible, the remaining pixels used only the 1200^{o}C blackbody. It is not possible to solve for SR using Eqn. 8 and only one blackbody temperature. Thus, another spectral responsivity approximation omits the unknown k because the 1200^{o}C blackbody signal-to-noise dominates any unknown spectral contributions.

$$SR = \frac{S}{F\eta e^{-\tau}[B_h A\Omega]} \tag{10}$$

Using the spectral responsivity determined through the two temperature method, equations 8 and 9 can be solved for k. This unknown should represent the contributions to the spectra that are not accounted for in Eqn. 6. The result of the calculation is shown in Fig. 13 with the flat room temperature blackbody source plotted in the background (light grey). The unknown spectral contribution, k, is seen to be essentially flat and thus will not change the shape of the spectral responsivity, as measurements occur in the Rayleigh-Jeans region.

5.4. Comparisons across PLW Array

As seen in Fig. 11, the spectral responsivities from different pixels are in general agreement. The low and high frequency cutoffs are unvarying. Spectral profiles agree, however, the normalization factors are not fully understood. Post-vibration CQM testing is expected to investigate this further.

6. CONCLUSIONS

The TFTS performance has been validated. The molecular laser measurements show that the TFTS exceeds its design specifications. The basic SPIRE instrument function was verified. The operating range of the PLW array matches well with the design criteria. Furthermore there is no evidence of any out-of-band spectral leaks. The shape of the PLW array spectral responsivity is not yet fully understood. The cause of this has not been determined, some factors associated with apodisation or multiple reflections have been eliminated due to the tests performed with the laser. The spectra of all pixels are in general agreement with each other, however, the profile shape and intensity variations are not yet fully understood.

Furthermore, the experience gained testing the PLW array allows us to predict, with some confidence, the expected spectral profile from the testing of the other four SPIRE arrays.

The post-vibration test schedule is similar to the pre-vibration schedule, but will probe some areas further.[4] The TFTS performance has been well established, so future spectral scans can concentrate on SPIRE internal

investigations and verifying more pixels. In addition to the pixels tested in the pre-vibration test campaign, the post-vibration test will also observe performance of pixels B3, B7, D3, D7 (Fig. 5). The test Fourier transform spectrometer has proven to be a valuable piece of test equipment in the SPIRE test laboratory.

ACKNOWLEDGMENTS

The authors wish to thank Professor G.R.Davis, now Director of the James Clerk Maxwell Telescope, for negotating and securing approval for Canada's participation in the SPIRE project. This work would otherwise not have been possible.

The authors also wish to thank the following for their help: Peter Ade,Ian Chapman, Peter Davis, Kris Dyke, Marc Ferlet, Nathan Fitzpatrick, Doug Griffin, Matt Griffin, Steve Guest, Ken King, Sarah Leeks, John Lindner, Judy Long, Kristie Masuda, Alan Pearce, Berhard Schulz, Sunil Sidher, Dave Smith, Margaret Tahic, Greg Tompkins, Mike Trower. This research is funded in part by grants from CIPI (LDS), CSA (AAA, TRF, DAN, SDR, ISS, LDS), and NSERC (DAN). The SPIRE instrument development in the UK is funded by PPARC.

REFERENCES

1. G. L. Pilbratt, "Herschel Mission: status and observing opportunities," *Optical, Infrared, and Millimeter Space Telescopes, Proc. SPIE* **5487**, Jun 2004.
2. G. L. Pilbratt, "The ESA FIRST cornerstone mission," *UV, Optical, and IR Space Telescopes and Instruments, Proc. SPIE* **4013**, pp. 142–151, Mar 2000. SPIE symposium, 29-31 March 2000.
3. B. Swinyard, K. Dohlen, D. Ferand, J. P. Baluteau, D. Pouliquen, P. Dargent, G. Michel, J. Martignac, P. Ade, P. Hargrave, M. Griffin, D. Jennings, and M. Caldwell, "The Imaging FTS for Herscel SPIRE," *IR Space Telescopes and Instruments, Proc. SPIE* **4850**, pp. 698–709, Mar 2003.
4. T. Lim, B. Swinyard, A. A. Aramburu, J. Bock, M. Ferlet, D. Griffin, M. J. Griffin, P. Hargrave, K. King, S. Leeks, S. ROnayette, E. Sawyer, B. Schulz, S. Sider, D. Smith, and L. Spencer, "First Results from Herschel/SPIRE performance tests," *Optical, Infrared, and Millimeter Space Telescopes, Proc. SPIE* **5487**, Jun 2004.
5. M. J. Griffin, B. M. Swinyard, and L. Vigroux, "The Herschel: SPIRE instrument," *Optical, Infrared, and Millimeter Space Telescopes, Proc. SPIE* **5487**, Jun 2004.
6. K. Dohlen, A. Origne, and M. Ferlet, "Optical alignment verification of the Herschel-SPIRE instrument," *Optical, Infrared, and Millimeter Space Telescopes, Proc. SPIE* **5487**, Jun 2004.
7. P. A. Collins, P. A. R. Ade, M. Caldwell, M. Ferlet, M. J. Griffin, P. C. Hargrave, M. R. Harman, D. L. Smith, and B. M. Swinyard, "A Ground Calibration Facility for Herschel-SPIRE," *IR Space Telescopes and Instruments, Proc. SPIE* **4850**, Mar 2003.
8. M. Griffin, B. Swinyard, and L. Vigroux, "The SPIRE instrument for FIRST," *UV, Optical, and IR Space Telescopes and Instruments, Proc. SPIE* **4013**, pp. 184–195, Mar 2000. SPIE symposium, 29-31 March 2000.
9. S. P. Davis, M. C. Abrams, and J. W. Brault, *Fourier Transform Spectroscopy*, Academic Press, first ed., 2001.
10. F. Pinsard, "Herschel/SPIRE Detector Control Unit Design Document," Tech. Rep. SPIRE-SAP-PRJ-001243, Rutherford Appleton Laboratories, Feb 2003.
11. I. Chapman, "The Atmosphere Above Mauna Kea at Mid-Infrared Wavelengths," Master's thesis, University of Lethbridge, Lethbridge, Canada, Dec 2002.
12. http://fits.gsfc.nasa.gov/fits_intro.html.
13. K. Dyke, P. Davis, D. Naylor, T. Fulton, I. Chapman, L. Spencer, and J. Lindner, "University of lethbridge data processing toolkit architecture design document," tech. rep., Astronomical Instrumentation Group, University of Lethbridge, 2003.
14. "Interactive Data Language, Research Systems Inc.," 2003.
15. R. J. Bell, *Introductory Fourier Transform Spectroscopy*, Academic Press, New York, 1972.
16. Jet Propulsion Laboratory, California Institute of Technology, CA, USA.
17. Laboratoire d'Astronomie Spatiale, Marseille, France.
18. "LabVIEW, www.ni.com, National Instruments Inc.."